Energy Conversion and Management: X 6 (2020) 100039

Contents lists available at ScienceDirect

Energy Conversion and Management: X

journal homepage: www.journals.elsevier.com/energy-conversion-and-management-x

Integration of thermochemical energy storage in concentrated solar power. Part 1: Energy and economic analysis/optimization

U. Tesio[a,*], E. Guelpa[a], V. Verda[a]

[a] Energy Department, Politecnico di Torino, Turin, Italy

ARTICLE INFO

Keywords:
Calcium-Looping
Indirect integration
Techno-economic analysis
Cost function
High temperature
Sustainability

ABSTRACT

Coupling of Concentrated Solar Power and Thermo-Chemical Energy Storage is a very interesting option because of the high efficiencies attainable with a renewable source and the large variation of solar radiation. Thermo-Chemical Energy Storage based on Calcium-Looping represents a promising opportunity thanks to high operating temperature, high energy density, null thermal losses and cheap calcium oxide precursor exploitable. The large variety of suitable power blocks and the importance of their integration in the discharging process makes it necessary to perform a coherent analysis of the selected alternatives, in order to compare them and establish the most convenient integration. Many aspects must be taken into account, such as system efficiency, investment costs and layout complexity. The purposes of the present work are: the development of a methodology to simulate the entire plant operations; the synthesis of heat recovery systems for both the charging and discharging processes; the execution of an economic analysis and the development of economic optimizations for the design/dimensioning of solar side and calciner side. Between the options investigated, power blocks based on supercritical CO_2 are the most convenient both in terms of global efficiency (higher than 19%) and capital investment, keeping this advantage also for higher plant sizes. The methodology here developed and the results obtained are useful information for a deeper analysis of the most promising integration alternative, which is performed in the second part of this study.

1. Introduction

Most of the international energy policies [1,2] adopted in the last decades have the objective of consistently enhancing the use of renewable sources in order to contain the global warming [3] and reach a sustainable alternative for energy production. Concentrated Solar Power (CSP) plays an important role in this field since it represents a relatively cheap option for heat storage [4,5], allowing to overcome the issue of the intermittency that characterize the solar radiation. Despite Parabolic Through Concentrator (PTC) is more widespread at the present [6], central tower CSP attracts considerable interest [7] because of the high temperatures exploitable. There is a great variety of Thermal Energy Storages (TES) that can be integrated in the plant [8], which are based on sensible heat (mostly with molten salts [9-11]), latent heat [12] or heat of chemical reaction [13]. Many researches are recently performed on this last technology [14-16] because of the absence of storage thermal losses [17]. The reversible reaction involving calcium oxide (Calcium-Looping) is one of the most interesting alternatives due to a) its high discharging temperatures [18], b) high energy density [19] and c) exploitation of an abundant and cheap material as $CaCO_3$ [20]. A further noticeable aspect, according to operating conditions, is the possibility of discharging the heat previously stored at a temperature higher than the one reached in the solar receiver [21].

$$CaCO_{3(s)} + HEAT \leftrightarrow CaO_{(s)} + CO_{2(g)} \Delta h_r^0 = \pm 178 kJ/mol \quad (1)$$

$$T_{eq} = -\frac{20474}{\ln\left(\frac{P_{CO_2}}{4.137 \cdot 10^7}\right)} \quad (2)$$

Eq. (1) shows the reversible chemical reaction exploited in the CaL process (Δh_r^0 is the molar heat of reaction for the standard conditions). The endothermic process is called calcination, it takes place in the solar calciner and is driven by the heat flux coming from the heliostat field, while the exothermic reaction is the carbonation and is carried out in the carbonator reactor. In Eq. (2) is reported the equilibrium temperature (in K) as a function of the CO_2 partial pressure (in bar) and allows to determine the direction in which the reaction takes place spontaneously [22]. One important drawback related to this process is due to the non-ideal process reversibility [23]; the parameter that provides a measurement of this phenomenon is the CaO conversion (or activity, X) and is obtained as the ratio between the calcium oxide

* Corresponding author.
E-mail address: umberto.tesio@polito.it (U. Tesio).

https://doi.org/10.1016/j.ecmx.2020.100039
Received 23 December 2019; Received in revised form 9 February 2020; Accepted 12 February 2020
Available online 03 March 2020

Nomenclature

Nomenclature and letters

A	Heat exchange area, m^2
c	Specific cost
$CaCO_3$	Calcium carbonate
CaO	Calcium oxide
CO_2	Carbon dioxide
c_p	Specific heat capacity, J/(kg·K)
d	Diameter, m
h	Specific enthalpy, J/kg
H	Height, m
l	Length, m
$\dot{m}$	Mass flowrate, kg/s
M	Mass, kg
n	Moles number
P	Pressure, bar
Q	Heat, J
S	Allowable stress, MPa
T	Temperature, K
t	Time, s
U	Global heat transfer coefficient, W/(m^2·K)
V	Volume, m^3
$\dot{W}$	Power flux, W
X	CaO conversion
Y	Yeld stress, MPa

Abbreviations

CaL	Calcium-Looping
CC	Combined Cycle
CCS	Carbon Capture and Storage
CIP	Compressor inlet pressure, bar
CIT	Compressor inlet temperature, K
COP	Compressor outlet pressure, bar
CPC	Compound Parabolic Concentrator
CSP	Concentrated Solar Power
DNI	Direct Normal Irradiation, W/m^2
EF	Entrained Flow
FB	Fluidized Bed
HEN	Heat Exchangers Network
HEX	Heat exchanger
HTR	High Temperature Regenerator
IC	Investment cost, $
LTR	Low Temperature Regenerator
ORC	Organic Rankine Cycle
PTC	Parabolic Trough Collector
sCO_2	Supercritical CO_2
SRC	Steam Rankine Cycle
TCES	ThermoChemical Energy Storage
TES	Thermal Energy Storage
TIT	Turbine inlet temperature, K
VG	Vapor Generator

Greek letters

Δ	Difference
β	Pressure ratio
δ	Thickness, m
η	Efficiency
ρ	Density, kg/ m^3
φ	Thermal flux, W

Subscripts and superscripts

0	standard conditions
carb	carbonator
CarbS	Carbonator Side
clc	calciner
ClcS	Calciner Side
comp	compressor
des	design
EG	Electricity Generator
el	electric
eq	equivalent
H	Heater
helio	heliostat field
in	inlet/inner
is	isentropic
lm	logarithmic mean
MIN	minimum
out	outlet
out	outlet/outer
PB	Power Block
r	reaction
ss	Stainless steel
stor	storage
tot	total
tow	tower
turb	turbine
un	unreacted

converted into $CaCO_3$ and the total amount of CaO provided to the carbonator reactor.

Until the last years, the main field in which Calcium-Looping has been investigated is the Carbon Capture and Sequestration performed on the flue gases of fossil-fuel power plants [24,25]; however, if compared to its integration in CSP [26], the operating conditions occurring in this context penalizes consistently the CaO conversion, posing a considerable limitation to its convenience both in energy and economic terms.

The Thermo-Chemical Energy Storage (TCES) based on Calcium-Looping can be both directly or indirectly integrated in a central tower CSP plant; the differences are exclusively related to the discharging phase. In the first case the power fluid enters the carbonator and directly absorbs the heat released by the exothermic reaction; the successive expansion in a turbine allows to convert this thermal energy into electricity. The thermodynamic cycles adopted in this case are two: closed CO_2 and open air/CO_2 Brayton cycles. Optimal operating conditions for the former one with energy storage at ambient temperature are investigated in [27], [28] and [29] through both pinch analysis [30] and sensitivity analysis, while the plant discharge phase optimization with the HEATSEP method is presented in [31]. The addition of a Rankine cycle fed by the calciner CO_2 outflow and high temperature solids storage is studied in [32]. The resulting configurations are encouraging both in terms of efficiency and non-critical operating conditions. Open air/CO_2 Brayton cycle is investigated in [33] but, although its good performance, the drawback of carbon dioxide emission in the ambient affects the plant functioning because of the execution of carbonation under a non-pure CO_2 reactor atmosphere.

The indirect integration includes a separate power block. The thermal power is provided through a heat exchanger; this allows a higher degree of freedom in the choice of the power fluid and the pressures reached in the cycle. Rankine cycle, supercritical CO_2 Brayton

cycle and combined cycle are analyzed in [29] as possible candidates for this kind of integration. Despite the sCO2 power block reaches the highest efficiency, it results to be the least performing option when integrated in the CaL process; however, in this case it is assumed that the thermal cycle is fed only by the gaseous carbonator outflow. The convenience in energy terms between the two possibilities is evaluated in [34], where the best option is direct integration (closed CO_2) or indirect integration (simple Rankine cycle) depending on the operating conditions.

A comparison of the works found in literature about this topic is provided in [35] with the addition of interesting comments.

For a power plant, the convenience in terms of investment cost can be as crucial as its energy performance; for this reason is fundamental to include the economic aspect in the analysis. Several studies are present in literature in which the economic analysis is conducted for the case of CaL employed in CCS plants [36–39], while its application as TCES for the electrical surplus coming from the photovoltaic is investigated in [40] both in efficiency and investment costs terms. However, to the authors knowledge, a complete economic study carried out for the CaL integration in the CSP field is lacking.

The purposes of this work are to develop a model for the calciner side simulation and dimensioning, taking into account the strictly time dependence of this plant portion. The final aim consists in evaluating the economic convenience of different power blocks indirectly integrated in the TCES based on Calcium-Looping of a central tower CSP pilot plant. To do that, suitable solution to technical issues affecting the heat exchange processes must be provided. This study provides a first selection of the most interesting alternatives for the power production and includes useful informations to establish the direction of further researches.

The novelties of the present study are: i) the synthesis of the carbonator side Heat Exchanger Network for different power cycles whose integration has been optimized both in terms of plant efficiency and thermal transfer; ii) the heliostat field/calciner side optimization performed without the hypothesis of steady state conditions; iii) the complete plant investment cost for the CaL indirect integration in a CSP plant.

The paper structure is the following:

- Section 2: description of technology operation;
- Section 3: exposition of system simulation and optimization methodology;
- Section 4: discussion of economic analysis;
- Section 5: exposition of results obtained;
- Section 6: final comments and conclusions.

A companion paper (Part 2) is devoted to the deepening of the most promising integration found in the present paper, performing a multi-objective optimization with an increased number of layouts and power block feeding options investigated.

2. Case study

The indirect integration of a Calcium-Looping TCES in a central tower CSP plant is schematized in Fig. 1. Describing the system functioning is fundamental to understand the analysis performed in the present work. The charging process begins when the calcium carbonate (with the corresponding calcium oxide unreacted) is taken from the solid storage and preheated to be send to the solar calciner. Here the exothermic reaction decomposes the reactant into CO_2 and CaO, which are cooled down and sent back to the storages. To avoid excessive dimensions of the carbon dioxide vessel it is necessary to bring the gaseous stream up to 75 bar [27]; the electrical power consumption related to the compression process can be reduced with the insertion of intercooling stages.

In the discharging process the two reactants are extracted from their storages, preheated and sent to the carbonator reactor; here the opposite reaction releases the heat absorbed during the charging process. The stoichiometric carbon dioxide needs to be heated and expanded up to the carbonator pressure and, in order to control the adiabatic reactor operating temperature, an excess of CO_2 must be provided to the reactor and successively recirculated. The carbonator products are therefore cooled down and the solid stream can be returned to the storage. It is important to notice that keeping the storages at ambient temperature makes possible to avoid any thermal loss due to the non-ideal vessels insulation. The power block (represented in a simplified form in Fig. 1) is thermally fed recovering part of the sensible heat of the reaction products. Using an indirect heat exchange, the thermodynamic cycle operation can significantly differ from the carbonator side conditions, especially in terms of maximum achievable pressures, and the reactor atmosphere can be set equal to the ambient pressure [32].

Taking into account the operating conditions attainable in the carbonator, the power block options for the indirect integration are:

1) high-temperature Organic Rankine Cycles (ORC);
2) Steam Rankine Cycles (SRC);
3) Brayton-Joule cycles;
4) Combined Cycles (CC);
5) Stirling cycles.

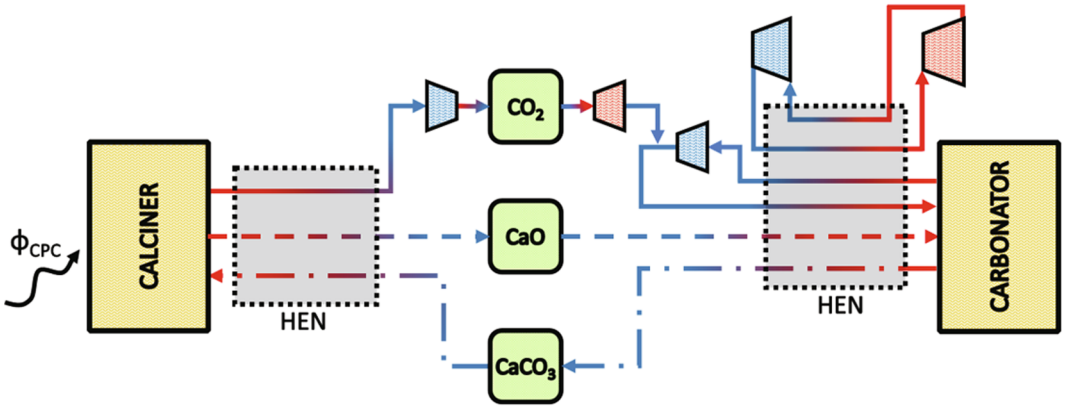

Fig. 1. Conceptual scheme of Calcium-Looping indirect integration.

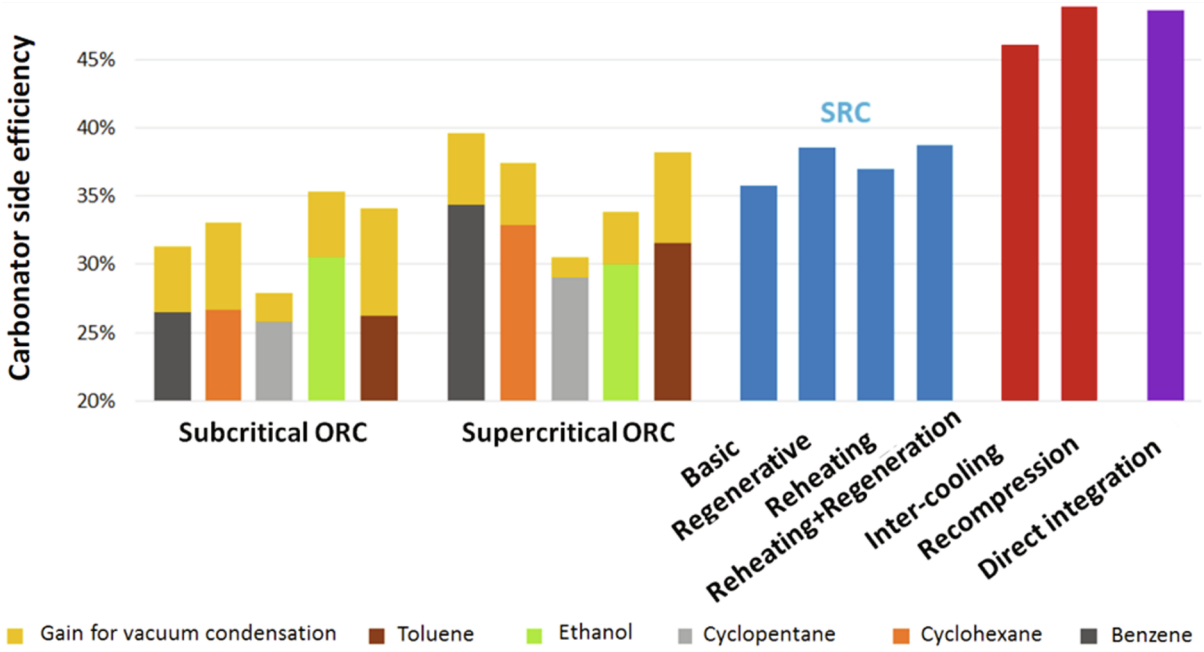

Fig. 2. Discharge process efficiencies for several thermal cycles [17].

As reported in [17], reaching a Technology Readiness Level (TRL) equal to 5 is one of the objectives at short term for this kind of technology. This means that, at the state of the art, the system is still far from being developed on a commercial scale. For this reason, power blocks with a net electrical output of 1 MW are assumed. Combined cycles and Stirling cycles are the less suitable options for the purposes of this study since the plant size is too small for a CC and too big for a single Stirling engine [41]; for these reasons their integration is not analyzed.

The present work starts from the optimized carbonator conditions found in [42] (Fig. 2). Very briefly, in that study the discharging process efficiency is maximized in two consecutive steps: 1) the thermodynamic cycle variables (temperatures, pressures or flow splits) are separately optimized to achieve the highest energy performances as possible; 2) the power block operating conditions are kept constant and its integration in the carbonator side is optimized both in terms of thermal transfer and primary components (turbomachinery and reactors) design parameters. This purpose is attained with the HEATSEP method [43], whose execution exploits pinch analysis, genetic algorithm and bisection as nested optimization methods. Suitable constraints are imposed to avoid the use of external heating sources making this plant 100% renewable and to satisfy the technical limitations. The power fluids, the operating conditions and the thermodynamic cycle layouts investigated for the indirect integration are summed up in Table 1; to reduce the analysis extension, only two cases are assumed for the Organic Rankine Cycles, which are the most interesting types for the subcritical and supercritical configurations. Despite their lower efficiency in stand-alone configuration, ORCs are considered because of two reasons: i) the show much better performances once they are integrated in the carbonator side; ii) evaluate in economic terms the advantages brought by their interesting thermal properties (e.g. smaller heat exchangers).

Table 1
Power blocks considered in the analysis.

Power fluid	Operating conditions	Layout
Ethanol	Subcritical + vacuum condensation	Basic
Benzene	Supercritical + vacuum condensation	Basic
Water	Subcritical	Regenerative
		Regenerative and reheated
Carbon dioxide	Supercritical	Inter-cooled Recompression

3. Plant simulation/optimization

To perform the complete CSP plant economic comparison, which is the main aim of the present study, it is necessary to complete the optimized results taken as input [42]. The following subparagraphs (3.1–3.4) are devoted to the discussion of all the steps with the whom is possible to reach this scope. In particular, in subparagraph 3.3 is included the exposition of the calciner side HEN layout obtained from pinch analysis. This is done in order to make more understandable the explanation of the economic analysis and the related considerations.

As investigated in [42] with a sensitive analysis, the performance of discharging process decreases for lower values of CaO conversion. For most of the CaL integrations considered in this study, carbonator side efficiency decreases of two decimals when X passes from 0.5 to 0.2. In addition, lower values of X determine higher sizes of heat exchangers (because of the presence of inert matter), solar calciner and heliostat field. Therefore, since low values of X contribute both increasing plant cost and decreasing performances, it is convenient to attain high CaO conversion. According to studies performed on CaO precursors in multicyclic conversions [20,21], a value of X equal to 0.5 is assumed.

To evaluate the performance of the different sections constituting the plant are used some benchmarks. Carbonator side efficiency is computed with Eq. (3) and represents the stand-alone power cycle performance ($\Phi_{H_1+H_2}$ is the total heat flux absorbed by the heaters belonging to the power cycle). Calcium-Looping efficiency is obtained with Eq. (4) and quantifies the system performance at the net of heliostat field, Compound Parabolic Concentrator and solar calciner losses. Finally, the total plant efficiency is obtained with Eq. (5).

$$\eta_{PB} = \frac{\dot{W}_{el,PB}}{\Phi_{H_1+H_2}} \tag{3}$$

$$\eta_{CaL} = \frac{E_{el,tot}}{Q_{clc,net}} = \frac{\int_{day}^{off} (\dot{W}_{el,CarbS}(t) + \dot{W}_{el,ClcS}(t))dt}{\int_{on} \eta_{helio}(t)\eta_{CPC}\eta_{clc}A_{helio}DNI(t)dt} \tag{4}$$

$$\eta_{tot} = \frac{E_{el,tot}}{Q_{sol}} = \frac{\int_{day} (\dot{W}_{el,CarbS}(t) + \dot{W}_{el,ClcS}(t))dt}{\int_{day} A_{helio}DNI(t)dt} \tag{5}$$

3.1. Carbonator side heat exchanger network

All the data used for the design of the carbonator side HEN are provided in [42]. Its synthesis is performed trying to satisfy, whenever possible, two suggestions [28]: first, avoid thermal transfer between solids and, second, avoid splitting solid streams. Both of them are aimed to reduce the technical complexity occurring during the plant operation.

Taking the regenerative Steam Rankine Cycle as an example, the fluids involved in the heat exchange process and the hot and cold composite curves are shown in Table 2 and Fig. 3. These same data referred to all the other indirect integrations considered (in addition to turbomachinery operating conditions) are the starting point of the present analysis.

The minimum temperature difference set in the pinch analysis is equal to 15 °C and ambient air at 20 °C is the cold source to which the process heat is released, performing therefore an air-cooling. Thermophysical properties used for the substances participating to the thermal transfer are taken from [44] for $CaCO_3$, [45] for CaO and for [46] for all the other fluids.

Table 2
Fluids data for pinch analysis (SRC is taken as an example).

Stream	Flowrate	T_{in}	T_{out}
$CaCO_3$ and unreacted CaO	2,77	875	20
Recirculated CO_2	1,72	875	139
CaO	1,99	20	310
Stoichiometric CO_2	2,50	20	650
H_2O	0,78	192	510

3.2. Tanks for material storage

The storage tanks mass dimensioning is conducted as follows: once the extracted and inserted CO_2 flowrates are found (as a function of time) thanks to the carbonator and calciner side simulation, the mass amount contained in the storage of the j-reactant ($M_{stor}(t)_j$) is calculated with the Eq. (6).

$$M_{stor}(t)_j = \int_{t_0}^{t} (\dot{m}_{in,j} - \dot{m}_{out,j})dt + M_{stor}(t_0)_j \tag{6}$$

where $\dot{m}_{in/out,j}$ is the inlet/outlet mass flowrate of the j-reactant and t_0 is the initial timestep assumed. The integral can be easily computed numerically. The initial amount of material present in the storage is obtained imposing the minimum M_{stor} acceptable value equal to zero (Eq. (7)).

$$\min(M_{stor}(t)_j) = 0 \rightarrow M_{stor}(t_0)_j \tag{7}$$

At this point the storage design volume is directly determined with Eq. (8).

$$V_{stor,j} = \max\left(\frac{M_{stor}(t)_j}{\rho_{stor,j}}\right) \tag{8}$$

Finally, is worth to mention the possibility to provide the solid reactants flowrates to the relative storages at a temperature close but not equal to the nominal value [27]. The storage vessels are not insulated, so the residual sensible heat goes dispersed to the environment, avoiding the addition of a dedicated air cooler.

3.3. Calciner side

The calciner side simulation and optimization can be conducted separately from the processes already discussed because any change occurring in the discharging phase does not have a direct influence on this plant portion: its operation is only influenced by the solar side. Therefore, at first some simplifying assumptions are made in order to take into account the strictly time dependent operations. Then, to optimize the calciner side, it is necessary to select the solar calciner typology. Falling particle receivers, centrifugal particle receivers, fluidized bed receivers and rotary kilns are possible candidates to the scope [28,35,47]. Considering the required operating conditions (calcination carried out under pure CO_2), the technology state of development and the data available on the literature, a rotary kiln reactor with a Compound Parabolic Concentrator (CPC) is assumed as solar calciner [48,49].

The assumptions used for the simulation of this plant section are summed up in Table 3; these values are taken from [32,34,50,51].

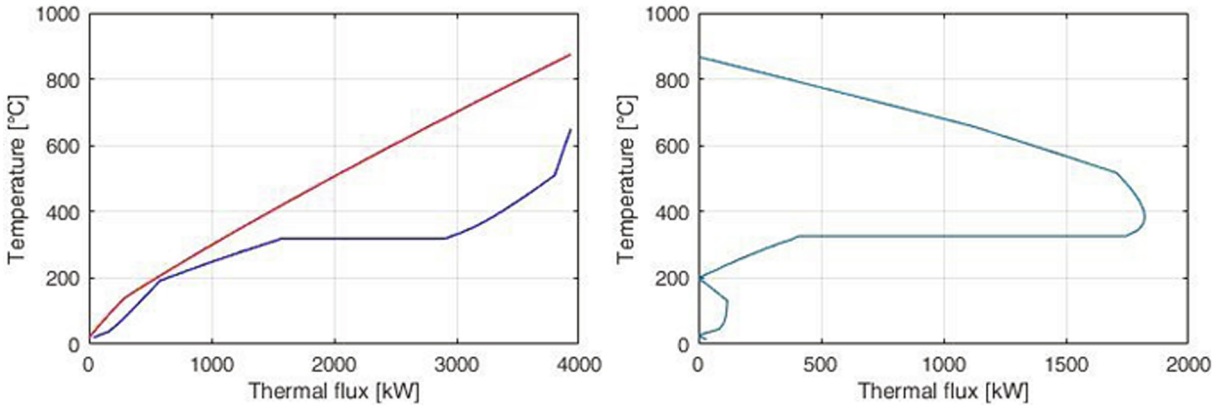

Fig. 3. Composite curves obtained from pinch analysis.

Table 3
Calciner side data assumptions.

Parameter	Component/stream	Value
Operating temperature	Calciner	950 °C
Cut-in power	Calciner	20% of calciner design power
Thermal losses	CPC	0.97
	Calciner	0.75
Isentropic efficiency	Compressors	0.8
Electrical efficiency	Electric motor	0.98
Compression intercooling stages	CO_2 compressor	5
Pressure losses	CO_2 coolers	1%
Solid conveying electrical consumption	CaO, $CaCO_3$	10 kJ/(kg·100 m)
Storages-calciner distance	CaO, $CaCO_3$	100 m
Heat rejection electrical consumption	Coolers	0.8% of rejected heat
Minimum ΔT	Gas-gas HEXs	15 °C
	HTF-solid HEXs	

For the solar calciner is adopted the model developed in [27], while the electric consumption due to the solid lift in the central tower can be estimated as indicated in [52]. However, after a preliminary check, this auxiliary requirement results negligible if compared to the power involved in the process; for this reason this has not been considered.

The calciner side energy optimization is performed with a fundamental simplifying hypothesis: the components operating parameters remain constant during the same operating period. Therefore, only the mass flow rates change proportionally to the solar radiation absorbed by the receiver, while pressures and temperatures across the layout do not vary. This allows using pinch analysis to optimize the calciner side layout, obtaining a HEN configuration that is suitable for the entire plant operations. The heat exchangers are dimensioned for the calciner side rated power (i.e. the nominal thermal flux to the receiver). For this reason, in case of lower heat inputs (and consequently lower flow rates), the HEN results oversized, leading to a more performing thermal transfer. The hypothesis of constant operating conditions for the Heat Exchanger Network is therefore precautionary and does not bring efficiency overestimations.

In order to minimize the consistent compression power (CO_2 must be brought for 1 bar to 75 bar), the addition of inter-cooling stages is recommended [27]. Significantly advantages are not encountered in the recovery of the heat generated by the compression, because of the low temperature at which is available, its relatively small amount and the complexity introduced in the layout structure. It is therefore assumed to release this heat to the ambient. According to [53,54], the compressors pressure ratio is imposed to be equal for all the stages, while the number of intercooling steps is subjected to the optimization process, as explained in the economic analysis chapter.

In the calciner side HEN is impossible to avoid the thermal transfer between solids, since there is only one cold stream to preheat and it is made of solid particles. For this reason it is necessary to use a Heat Transfer Fluid. The only imposed constraint is that the temperature differences at the HEX inlets/outlets must be equal. In this way, two heat exchangers with the same rated power and Logarithmic Mean Temperature Difference (ΔT_{ml}) are obtained, as shown in Fig. 4.

The resulting calciner side configuration is shown in Fig. 5, where the intercooled compression is synthetically represented with a single compressor and cooler. As explained in the following chapter, the $CaCO_3$ split ratio has no impact in energy terms but influences the HEN cost because of the change of ΔT_{ml} for the interested heat exchangers. Is therefore necessary to take into account this phenomenon in the economic analysis.

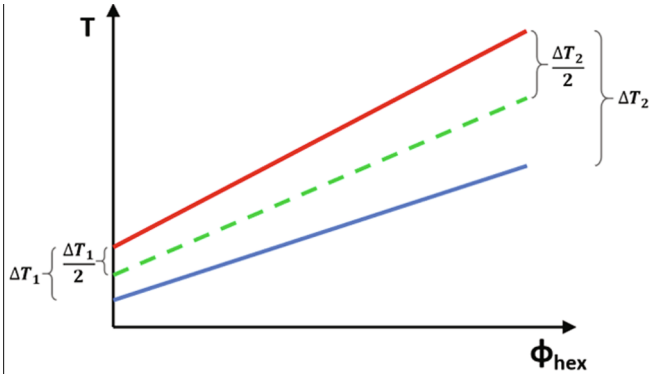

Fig. 4. Configuration assumed for indirect solids-solids thermal stransfer.

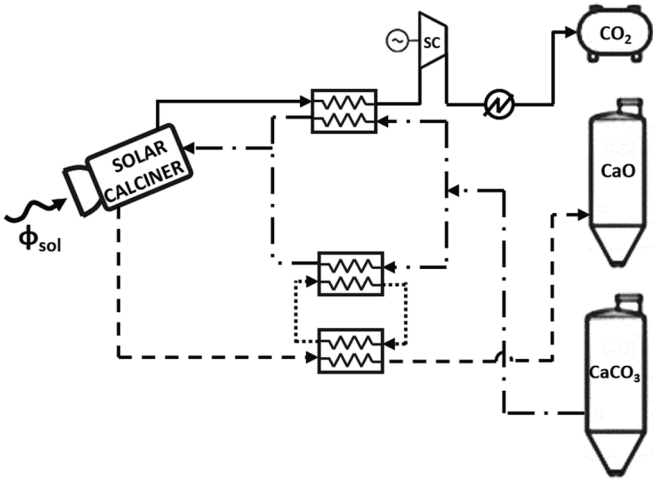

Fig. 5. Calciner side optimized layout.

3.4. Solar side

The solar side is simulated and optimized through a simplified approach. The winter solstice is set as the nominal day to dimension this plant portion in order to guarantee the power production imposed to the power block even in the most unfavorable day of the year. The plant location, the Direct Normal Irradiation (DNI) calculation and the heliostat field hourly efficiency (including atmospheric attenuation, mirrors reflection, shadowing and blocking, spillage and cosine losses) for a north-field are taken from [55] (DAHAN power plant).

The solar side is modelled as follow: from the carbonator side simulation is obtained the daily amount of $CaCO_3$ to be reconverted into CaO and CO_2 (with the relative CaO unreacted). Given the calciner reactants inlet temperatures, it is possible to compute the net thermal energy requested at the chemical reactor ($E_{clc,net}$) as the sum of chemical and sensible energy needs (Eq. (9)).

$$E_{clc,net} = n_{CaCO_3}\Delta h_r + M_{CaCO_3}\bar{c}_{p\,CaCO_3}(T_{clc} - T_{in,CaCO_3}) + M_{CaO_{un}}\bar{c}_{p\,CaO_{un}}(T_{clc} - T_{in,CaO_{un}}) \quad (9)$$

where n_{CaCO3} is the calcium carbonate moles number, Δh_r is the molar enthalpy of reaction at the calciner conditions, $M_{CaOun/CaCO3}$ is the unreacted $CaO/CaCO_3$ quantity in mass provided to the reactor, $\bar{c}_{p\,CaOun/CaCO3}$ is the corresponding average specific heat capacity, $T_{in,CaOun/CaCO3}$ is the calciner inlet temperature of the two substances and T_{clc} is the calciner design temperature.

The net thermal power employed to carry out the endothermic reaction $\Phi_{clc,net}$ is obtained with Eq. (10), where $\eta_{clc/CPC/helio}$ stands for the calciner/CPC/heliostat field efficiencies and A_{helio} is the total heliostats area.

$$\Phi_{clc,net}(t) = \eta_{clc}\cdot\eta_{CPC}\cdot\eta_{helio}(t)\cdot A_{helio}\cdot DNI(t) \quad (10)$$

According to [50], the minimum calciner net thermal power ($\Phi_{min,clc,net}$) is imposed as a fraction of the design calciner net heat flux ($\Phi_{des,clc,net}$); these values are the lower and upper bounds of the reactor operation (Eq. (11)).

$$\Phi_{min,clc,net} = 0.2\cdot\Phi_{des,clc,net} \quad (11)$$

The endothermic reaction starts at t_{on}, when the solar radiation overcomes the calciner minimum operating power and ends at t_{off}, when the thermal flux goes below the same limit. The reactor maximum achievable power is set equal to the design value; any power surplus provided by the heliostats is lost. As a consequence, the $E_{clc,net}$ can be written as shown in Eq. (12).

$$E_{clc,net} = \int_{t_{on}}^{t_{off}} \min\left(\Phi_{clc,net}(t)\,;\ \Phi_{des,clc,net}\right)dt = \int_{t_{on}}^{t_{off}} \min\left[\left(\eta_{clc}\cdot\eta_{CPC}\cdot\eta_{helio}(t)\cdot A_{helio}\cdot DNI(t)\right)\,;\ \Phi_{des,clc,net}\right)]dt \quad (12)$$

Concerning the evaluation of heliostat field area and calciner design power (highlighted in red in Eq.12), on an energy perspective these values are not unique and different configurations able to satisfy the reactor requirement ($E_{clc,net}$) can be found. However, their variation has a strong impact on the plant costs. A suitable optimization, discussed in the economic analysis chapter, is implemented in order to take into account this phenomenon.

Finally, is worth to comment some aspects related to the choice of the winter solstice as design day. Fig. 6 (referred to a value of $E_{clc,net}$ equal to $2*10^5$ MJ) shows the difference between winter and summer in terms of solar power availability. The area filled in light blue indicates the energy excess that the calciner would be able to absorb but that is lost because it overcomes the carbonator side disposal capacity. Possible ways to recover this energy are:

- Perform a storages oversize: reactants can be stored for more than 24 h and used during cloudy days;
- Reduce the carbonator side design operating time: the power block functioning can be extended over its nominal time during summer (storages oversize is also required);
- Calcination for alternative purposes: part of the $CaCO_3$ conversion can be exploited to produce CaO for the cement industry by means of a renewable source, with the avoidance of CO_2 emission (performing a CCS).

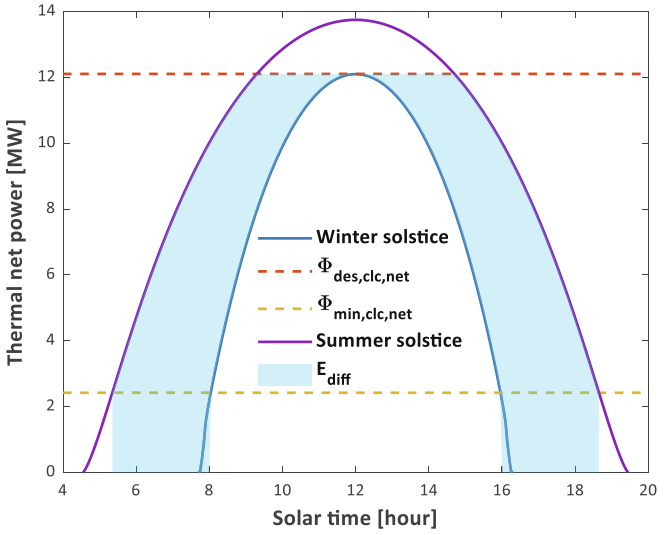

Fig. 6. Operation difference between winter and summer solstices in case of winter dimensioning.

4. Economic analysis

To the authors knowledge, in all the studies found in literature related to the CaL integration in a CSP plant, the energy analysis is the only kind of investigation performed. Very useful advice for the investment cost of the components involved in this application are provided in [35], while an economic analysis for a TCES based on CaL for the photovoltaic surplus production is carried out in [40]. The early stage of development of the investigated technology is the main obstacle for the economic study, since data based on real installations are poor or absent. In particular, the two chemical reactors are the components whose price can present the highest uncertainty. However, cost functions developed for the Carbon Capture and Sequestration field and lime industry allow to overcome this issue, providing a relatively good estimation since the operating conditions (pressures and temperatures) are not too different with respect to the case analyzed.

4.1. Estimation of components investment cost

For the purposes of the present work, the prices of the main components are considered and the total plant investment cost is calculated as the sum of those. Because of the absence of external sources consumption (such as fossil fuels) and the direct proportionality of annual costs (due to operating, maintenance and interest rates) to the total plant cost, it is possible to assume this last term as the parameter by which evaluate the economic convenience of a specific layout configuration. Costs functions and eventual procedures for the components investment cost estimation are listed below; all the prices are discounted to 2018 with CEPCI index and expressed in U.S. dollars. In case of currency exchange is assumed a €-$ rare equal to 1.18, referred to 2018 [56].

- ORC turbine cost is estimated by Eq. (13) (turbine shaft power in kW), taken from [57].

$$IC_{ORCturb} = 5050\cdot(\dot{W}_{turb})^{0.7} \quad (13)$$

- SRC turbine investment is provided to Eq. (14) as a function of inlet temperature (TIT [K]) and isentropic efficiency (η_{turb}) [57]; again, the scaling parameter is expressed in kW.

$$IC_{SRCturb} = 4125\cdot(\dot{W}_{turb})^{0.7}\left[1+\left(\frac{0.05}{1-\eta_{is,turb}}\right)^3\right]\left[1+\exp\left(\frac{TIT-866}{10.42}\right)\right] \quad (14)$$

- ORC pump price is calculated with Eq. (15), as suggested in [57] (machinery shaft power in kW).

$$IC_{ORCpump} = 213\cdot(\dot{W}_{pump})^{0.65} \quad (15)$$

- SRC pump investment cost is obtained with Eq. (16) (machinery shaft power in kW) [57].

$$IC_{SRCpump} = 750\cdot(\dot{W}_{pump})^{0.71}\left(1+\frac{0.2}{1-\eta_{is,pump}}\right) \quad (16)$$

- For sCO_2 turbines and compressors are adopted the power laws presented in [58] (Eq. (17) and (18)), where the scaling factor is the machinery shaft power (in kW).

$$IC_{SCO_2turb} = 8279\cdot(\dot{W}_{turb})^{0.6842} \quad (17)$$

$$IC_{SCO_2comp} = 7331\cdot(\dot{W}_{comp})^{0.7865} \quad (18)$$

- The costs of sCO_2 regenerators (HTR, LTR) and air coolers are obtained with Eq. (19) from the normalized cost value (c) calculated

Table 4
Normalized cost values for data interpolation.

	UA [W/K]	$5{\cdot}10^3$	$3{\cdot}10^4$	$1{\cdot}10^5$	$3{\cdot}10^5$	$1{\cdot}10^6$
c [$/(W/K)]	Regenerator	5,89	1,31	1,22	1,03	0,94
	Air cooler	9,66	3,05	1,65	1,40	1,27

through linear interpolation of the corresponding UA values (product between global heat transfer coefficient and exchange surface) with data in Table 4. This methodology is taken from [58] and is referred to the baselined case.

$$IC_{SCO_2 reg/cooler} = UA_{reg/cooler} \cdot c_{reg/cooler} \tag{19}$$

If the UA is higher than the maximum value reported in Table 4, c becomes constant and is set equal to its minimum corresponding value.

- Investment cost associated to CO_2 turbomachinery operating at subcritical conditions (storage compressor and turbine) is estimated with the methodology proposed in [59], exposed below in Eq. (20) and (21) (Turbine Inlet Temperature in K).

$$IC_{CO_2 turb} = \dot{m}_{eq,turb} \frac{492.2}{1-\eta_{is,turb}} \cdot \frac{TIP}{TOP_{eq}} \ln\left(\frac{TIP}{TOP_{eq}}\right)[1 + \exp(0.036 \cdot TIT - 65.66) \tag{20}$$

$$IC_{CO_2 comp} = \dot{m}_{eq,comp} \frac{59.1}{1-\eta_{is,comp}} \cdot \frac{COP_{eq}}{CIP} \ln\left(\frac{COP_{eq}}{CIP}\right) \tag{21}$$

The terms appearing with the subscript "eq" are referred to the thermo-physical value obtained in an equivalent case with air instead of carbon dioxide. The equivalent mass flowrate is computed with Eq. (22), while the equivalent outlet pressure is obtained through CoolProp data library for air, imposing $\rho_{eq,out}$ (Eq. (23)) and CO_2 outlet temperature.

$$\dot{m}_{eq,turb/comp} = \dot{m}_{turb/comp} \cdot \frac{\rho_{eq,in}}{\rho_{in}} \tag{22}$$

$$\rho_{eq,out} = \frac{\dot{m}_{eq,turb/comp}}{\dot{m}_{turb/comp}} \cdot \rho_{out} \tag{23}$$

- CO_2 blower cost in the carbonator side is calculated with Eq. (24), as proposed in [59] (blower shaft power is in kW).

$$IC_{blower} = 129520 \cdot \left(\frac{\dot{W}_{blower}}{445}\right)^{0.67} \tag{24}$$

- Electric generators prices are obtained with Eq. (25), assuming the electrical power output (in kW) as scaling parameter [59].

$$IC_{EG} = 106 \cdot (\dot{W}_{EG})^{0.95} \tag{25}$$

- For the purposes of this analysis, only two different types of heat exchanger are considered: fluid–fluid HEXs and fluid–solid indirect HEXs. Eq. (26) provides the investment estimation related to the former category [59], while, according to authors knowledge, cost functions suitable for the cases analyzed in the present work referred to the second type are not found in scientific literature. A proper function (Eq. (27)) is therefore extrapolated from the study of a gas–solid exchanger [60] that fulfills the cost target set in the DOE SunShot project [4]. For this purpose the same form of function is used. However, since the prediction of the global heat transfer coefficient in case of thermal transfer between fluids and solids is more difficult, the product UA (in W/K) is set as one of the scaling parameters instead of only the heat transfer surface (A, in m^2). In this way, besides the operating pressure (in bar), its investment cost is proportional to the thermal power exchanged and the Mean Logarithmic Temperature Difference.

$$IC_{fluid-fluidHEX} = 3197 \cdot A^{0.67} \cdot P^{0.28} \tag{26}$$

$$IC_{fluid-solidHEX} = 18.48 \cdot (UA)^{0.67} \cdot P^{0.28} \tag{27}$$

Heat transfer surfaces for fluid–fluid HEXs are computed assuming global heat transfer coefficients found in literature and reported in Table 5.

For the cooler/condenser dimensioning, the ambient air is assumed as heat sink with infinite thermal capacity.

- The price of the CO_2 vessel for the storage at 75 bar (Eq. (28)) is obtained with the procedure suggested in [62] for cylindrical pressure vessel; c_{SS} is the unit cost of Stainless Steel ($/kg), ρ_{ss} is the metal density (kg/m^3) and V_{ss} is the steel volume (m^3).

$$IC_{CO_2 storage} = c_{SS} \cdot \rho_{ss} \cdot V_{ss} \tag{28}$$

Fig. 7 represents schematically the CO_2 vessel and reports the dimensions necessary for its dimensioning.

Both the unit cost of Stainless Steel and the metal density are assumed according to [63] for 304L alloy, while the volume of metal constituting the vessel is calculated with Eq. 29–35.

$$V_{ss} = \pi(d_{out}^2 - d_{in}^2)(l_{out} + 2\delta_{ss}) + \frac{\pi(d_{out}^3 - d_{in}^3)}{6} \tag{29}$$

$$\delta_{ss} = \frac{P_{des} \cdot d_{in}}{4S \cdot E - 0.4P_{des}} \tag{30}$$

$$d_{in} = 0.22 \cdot l_{in} \tag{310}$$

$$l_{in} = \sqrt[3]{\frac{V_{storage}}{\pi \cdot \left(\frac{0.22}{2}\right)^2 + \frac{4}{3}\pi \cdot \left(\frac{0.22}{2}\right)^3}} \tag{32}$$

$$l_{out} = l_{in} + 2 \cdot H_{head} \tag{33}$$

$$H_{head} = 0.025 \cdot l_{in} \tag{34}$$

$$S = 0.9 \cdot Y \tag{35}$$

where $d_{in/out}$ is the inner/outer vessel diameter (m), l_{in} is the storage net length of the cylindrical section (m), l_{out} is its total cylindrical section length (m), H_{head} is the length of the safety joint between cylindrical body and spherical head (m), P_{des} is the design pressure (MPa), E is the joint efficiency (set to 0.9), S is the allowable stress (MPa) and finally, Y is the yield stress (MPa). The last two material properties are taken from [64].

- Two different cost functions are considered for the carbonator, according to the method of power block thermal feeding that is adopted. In case of adiabatic reactor and thermodynamic cycle fed with a heat recovery on the carbonator outflows, the component price is proportional to its volume, which depends on the inlet volume flowrate. It is therefore chosen the cost function proposed in [65] for entrained flow reactors (Eq. (36), $\dot{V}_{in}$ is in m^3). The function

Table 5
Global heat transfer coefficients for fluid–fluid HEXs.

HEX/fluids	U [W/(m^2K)]	Ref.
ORC VG	880	[57]
ORC regenerator	850	
SRC economizer	250	[61]
SRC evaporator	200	
SRC superheater	125	
CO_2 – CO_2	300	[59]
CO_2 – sCO_2	300	
ORC condenser	150	[57]
SRC condenser	150	
CO_2 air cooler	300	[59]

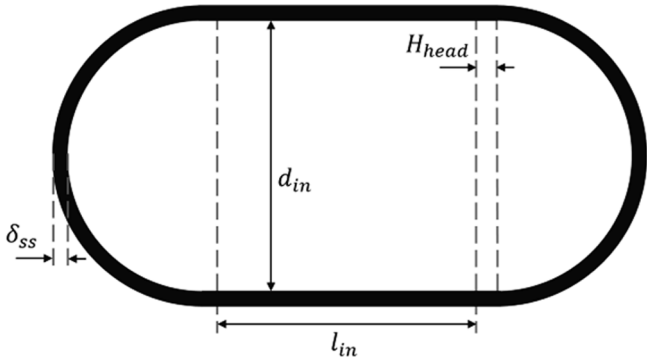

Fig. 7. Schematic of CO2 storage vessel with design dimensions.

presented in [59] for fluidized bed reactor is instead used when the SCO_2 thermodynamic cycle is fed with the heat of reaction on the carbonator walls, having as scaling parameter the reactor thermal power released by the carbonation (Eq. (37), Φ_{carb} in kW).

$$IC_{EFcarb} = 106200 \cdot (\dot{V}_{in})^{0.5} \quad (36)$$

$$IC_{FBcarb} = 19594 \cdot (\Phi_{carb})^{0.5} \quad (37$$

- Rotary kiln reactor with a Compound Parabolic Concentrator is the solar calciner typology assumed for the present analysis. Other alternatives are proposed in [27,32] but, at the state of the art, this type of reactor is chosen because it has reached a higher stage of development [35]. Investment costs related to these components (Eq. 38–40) are estimated as suggested in [50].

$$IC_{calc} = 533394 \cdot \left(\frac{\Phi_{clc}}{293}\right)^{0.48} \quad (38)$$

$$\Phi_{CPC} = \Phi_{clc}/\eta_{CPC} \quad (39)$$

$$IC_{CPC} = 37.56 \cdot \Phi_{CPC} + 57303 \quad (40)$$

Both the calciner gross power (Φ_{clc}) and the thermal flux on the CPC are expressed in kW, while η_{CPC} is the CPC efficiency. In addition, it is important to specify that, due to technical and operation constraints, the size of a single reactor cannot overcome the value of 55 MW [50]. The use of multiple solar calciners (of identical dimensions) must be therefore taken into account.

- For the evaluation of the central tower investment cost, Eqs. (41) and (42) are extrapolated from charts in [66]; H_{tow} is the tower height (m) and Φ_{CPC} is expressed in MW. Eq. (41) is referred to the case of north field arrangement. The tower price is computed with a piecewise function to take into account the change of its construction material (from steel to concrete) necessary to sustain the high stresses occurring in high towers.

$$H_{tow} = 15.67 \cdot (\Phi_{CPC})^{0.4849} \quad (41)$$

$$IC_{tow} = \begin{cases} 379 \cdot (H_{tow})^2 - 16370 \cdot H_{tow} + 1633200 H_{tow} < 122m \\ 287 \cdot (H_{tow})^2 - 43661 \cdot H_{tow} + 6338000 H_{tow} > 122m \end{cases} \quad (42)$$

- Heliostat field investment cost (Eq. (43) and (44)) is obtained through data fit of specific cost values presented in [67].

$$IC_{helio} = c_{helio} \cdot A_{helio} \quad (43)$$

$$c_{helio} = 3853 \cdot (A_{helio})^{-0.2976} \quad (44)$$

For the purposes of the present analysis, the power block thermal feeding is performed exploiting the sensible heat of the carbonator outflows. For this reason, an entrained flow chemical reactor is considered.

The plant specific investment cost (ic_{tot}) is the benchmark used to evaluate the economic convenience of the indirect integrations analyzed (Eq. (45)); this parameter is defined as the sum of the investment costs of the components divided by the electrical energy produced in the design day. This normalization is necessary because, despite the power block size is set to 1 MW for all the thermal cycles, the total plant production is different because of the contribution of the other turbomachinery involved in the CaL.

$$ic_{tot} = \frac{\sum_i [IC_i]}{E_{el}} \quad (45)$$

4.2. Economic optimization of charging process

In the following subparagraphs the assumptions and methodology used for the simulation and/or economic optimization are explained; this analysis is only related to the plant portions involved in the charging process. Results obtained from economic optimization of those system sections are here reported to make more immediate the comprehension of the analysis performed.

4.2.1. Tanks for material storage

The cost of the storages is mainly related to the pressurized CO_2 vessel. The CaO and $CaCO_3$ storages investment costs are assumed as negligible because of their small size (due to high solids density), the absence of thermal insulation (reactants at ambient temperature) and the gauge pressure equal to zero.

4.2.2. Calciner side

As already exposed, the calciner side heat recovery is optimized in energy terms through pinch analysis. The value of $CaCO_3$ split ratio is not unique and this influences the HEN investment cost; in fact it has an impact on the mean logarithmic temperature difference and consequently on the exchangers area. A suitable optimization is therefore needed to reach the minimum system price and to find the most convenient split value. Fig. 8 shows the HEN cost dependence on the split ratio and the solid flowrate for the whom it is obtained. The price variations observed in the selected range are consistent (up to 25%), demonstrating the optimization importance.

4.2.3. Solar side

With the equations provided in the previous chapter for the solar side and calciner side, it is possible to simulate the charging process. For first, the heliostat field area and the solar calciner rated power must be found. These parameters are not unique, since, on an energy point of view, they can assume different values that makes possible to provide the amount of reactants requested by the carbonation reaction. However, their impact on the investment cost and plant performance

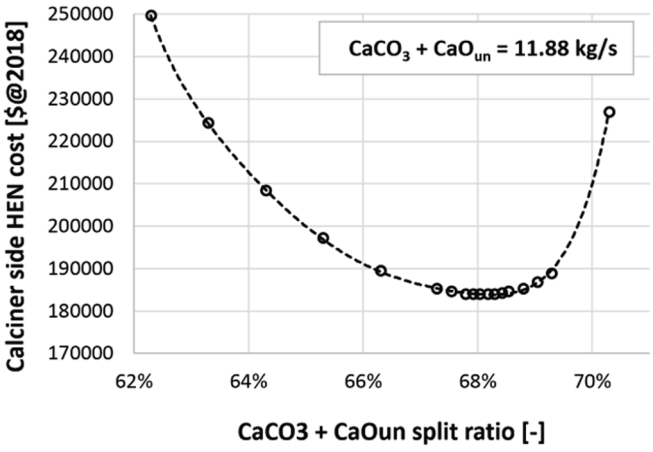

Fig. 8. Calciner side HEN investment cost as a function of solids split ratio.

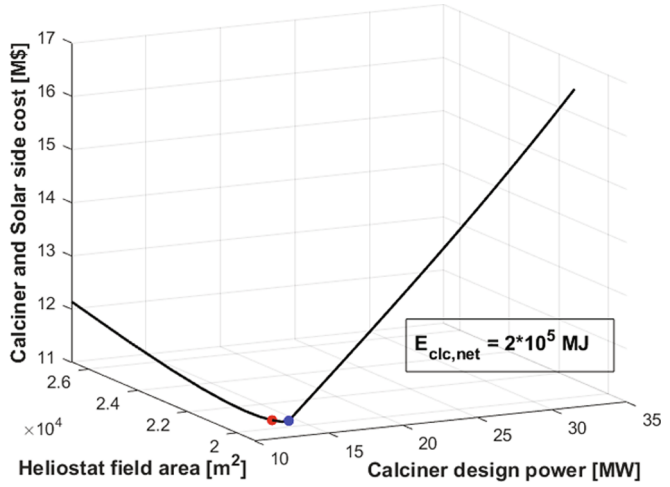

Fig. 9. Investment cost of charge plant section as a function of heliostat field and calciner sizes.

has to be assessed.

For a fixed amount of CaO and CO_2, the solar calciner size and heliostats area are inversely proportional: when the receiver nominal power decreases, the solar field area increases in order to extend the useful operating time and compensate the lower power that the reactor is capable to absorb (and vice versa). Considering this behavior, when the calciner side cost decreases, the solar side investment increases. At the same time, the most performing configuration in energy terms is the one with the minimum heliostat field area because exploits the lower solar radiation. However, it is not possible to establish a priori that this condition has the lowest investment cost and that, as a consequence, the energy and economic optimization coincide. For the purposes of the present study, the solar calciner size and heliostats area are dimensioned performing the economic optimization. The fminsearch algorithm (on MATLAB) is used for this purpose. To summarize the structure of the process just discussed, once that the discharging process is simulated and the amount of daily thermal energy requested at the solar calciner is computed, heliostat field area and calciner size are optimized in order to give a minimum investment cost and Eq. (12) is provided as equality constraint to satisfy.

Fig. 9 (obtained imposing $2{\cdot}10^5$ MJ as net thermal energy at the calciner) shows the sum of the solar side and calciner side capital investment as a function of the receiver nominal power and the solar field area. The blue and red points represent respectively the energy and economic optimization results; they are relatively close between them but they do not coincide, justifying the two optimizations performed.

The results obtained with this independent process are the optimal calciner design power and the solar field area, both as a function of the daily thermal energy requested to reverse the CaL reaction; in addition the design flowrates for the charge process are found. These data allow executing the discharging process simulation and a coherent optimization of the total plant.

Being both dependent on the same parameter, it is possible to couple the values assumed by the two optimized variables; the result is presented in Fig. 10a. The relation between these measures becomes non-smooth in correspondence of two particular conditions:

1) When the solar power reaches a value that is a multiple of the maximum calciner achievable size. In this case, to retard as much as possible the introduction of a new reactor (and therefore its drawback on the prices), it is convenient to keep constant the receiver size and increase only the heliostat field area.
2) When the height reached by the central tower requires the change of its construction material (from steel to concrete). The different slope assumed by the corresponding cost function in this restricted region makes convenient increasing only the receiver size and maintain the solar field area constant.

Finally, the investment cost related to the components involved in the charging process is shown in Fig. 10b as a function of the net thermal energy exploited by the solar calciner. Even in this chart, the two sudden changes in the total price due to the addition of another reactor are immediately recognizable, while the transition from steel to concrete tower structure has such a low impact that is not possible to notice it.

5. Comparison of indirect integrations

The three efficiencies that mostly affect the system operations obtained from the complete plant simulation are presented in Fig. 11. It is interesting to notice that, except for the case of intercooled sCO_2 (due to the absence of regeneration initially assumed), a higher thermodynamic cycle efficiency brings to higher CaL and plant efficiencies, highlighting the consistent influence that the power block performance has on the

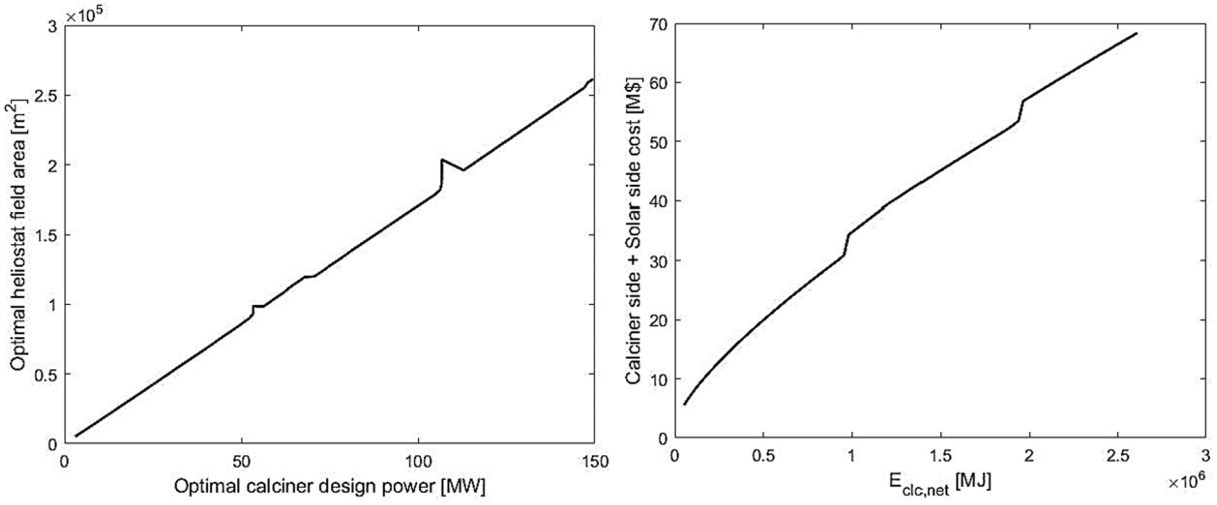

Fig. 10. Optimal sizes of heliostat field and solar calciner (a) and investment cost of charge plant section as a function of the net energy required by carbonator side (b).

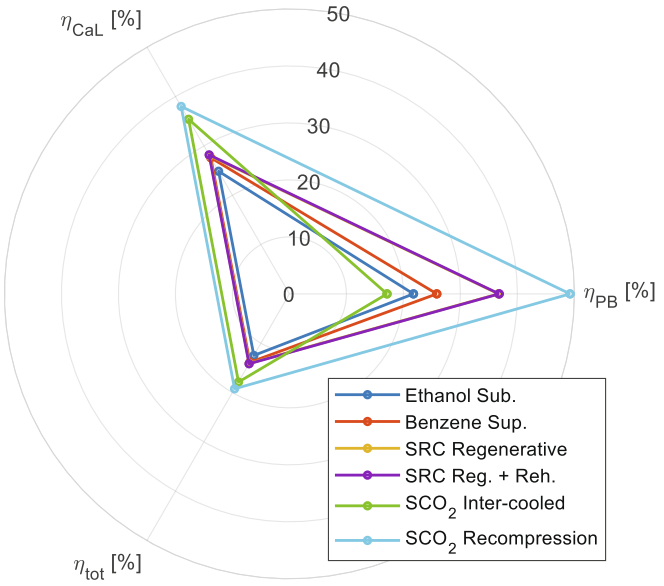

Fig. 11. Energy performance for different plant sections: power block efficiency (η_{PB}), Calcium-Looping efficiency (η_{CaL}) and total plant efficiency (η_{tot}).

Table 6
HEXs number for carbonator side.

Power block	Carbonator side HEXs number
Ethanol	11
Benzene	13
SRC reg.	8
SRC reg. + reh.	9
sCO_2 i.c.	12
sCO_2 rec.	12

system operation. The steam Rankine cycles are nearly overlying, which means that the presence of a reheating stage does not constitute an issue for its integration in the carbonator side.

The number of heat exchangers resulting from the carbonator side HEN design is reported in Table 6 (thermal cycles regenerators are not included). Steam Rankine cycles present the simplest layouts, while ORCs and sCO_2 integration complexity is practically the same. Solid stream splits are avoided only in case of intercooled sCO_2, while it is not possible to avoid thermal transfer between solid streams with SRCs and recompressed sCO_2; however, this last fact does not constitute an issue for the system operation since the heat exchangers sizes are actually small.

The indirect integrations are compared in economic terms in Fig. 12. Broadly speaking, the specific investment cost results inversely proportional to the plant efficiency; as a consequence, supercritical CO_2 power blocks are the best alternative found with the economic analysis. Taking the intercooled sCO_2 integration as reference, specific investment costs for steam Rankine cycles are about 3% higher (in relative terms) and even worse for organic Rankine cycles (7% for benzene and 11% for ethanol).

Another interesting result can be observed in Fig. 13. Despite the intercooled sCO_2 indirect integration is the option with the lowest specific investment cost, its total plant cost is not the lowest. Since sCO_2 power block with recompression layout is the most performing in energy terms and requires the lowest capital investment, it could be expected to be the most convenient in economic terms. However, it must be taken into account that the power generated at the carbonator side (electric generator connected to storage turbine and CO_2 blower) is lower with respect to the other layout analyzed for the supercritical

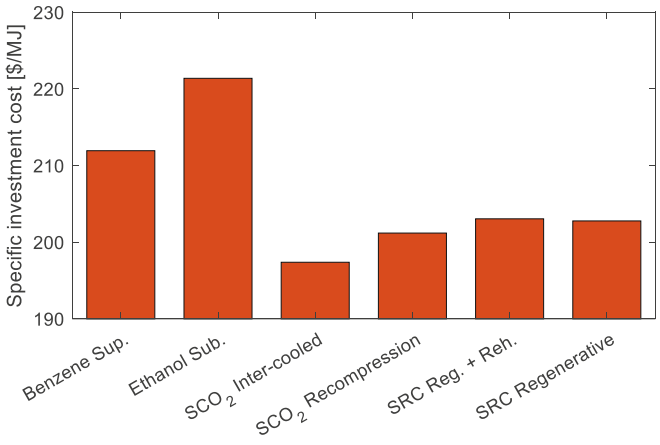

Fig. 12. Specific investment costs for analyzed configurations.

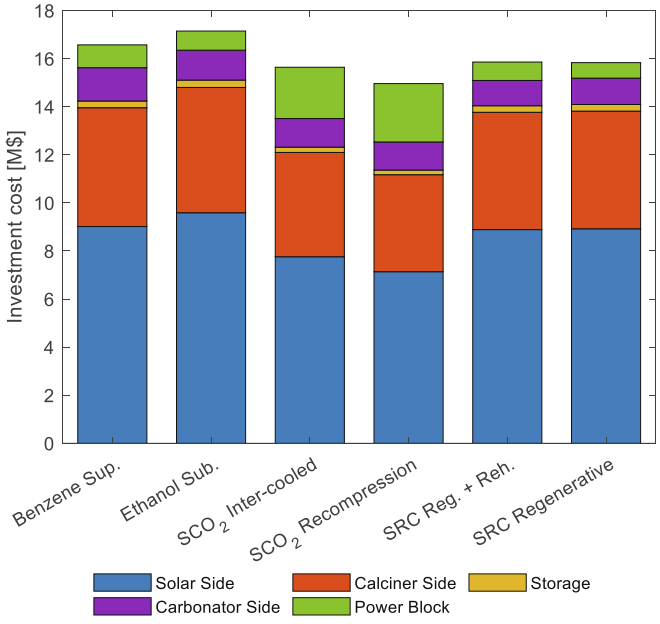

Fig. 13. Investment costs of the different plant sections.

carbon dioxide. Consequently, the net daily energy output of the intercooled layout results higher and its economic convenience is enhanced.

The same figure highlights the contributions of each plant section to the total capital investment. Costs associated to the charge plant portion (solar side and calciner side) are by far the most consistent (from 75% to 86% of the plant price) and they are directly influenced by the discharging process efficiency. Therefore, reducing this part of the investment is crucial for the economic convenience of the system. The only way to attain this purpose is to exploit an efficient thermodynamic cycle. However, it must be noticed that sCO_2 power blocks are much more expensive (nearly three times) if compared to both organic and steam Rankine cycles; the costs increase determined by the adoption of sCO_2 layouts with a high number of turbomachinery and/or regenerators can reduce the advantages obtained from the decrease of prices associated to the charge plant section. From a separate calculation is obtained that sCO_2 recompression configuration results to be still competitive with SRCs even if turbomachinery investment cost rise by 5.7%. Therefore, possible uncertainties affecting the price estimation of this novel technology do not change the results of the present economic analysis if contained in this range.

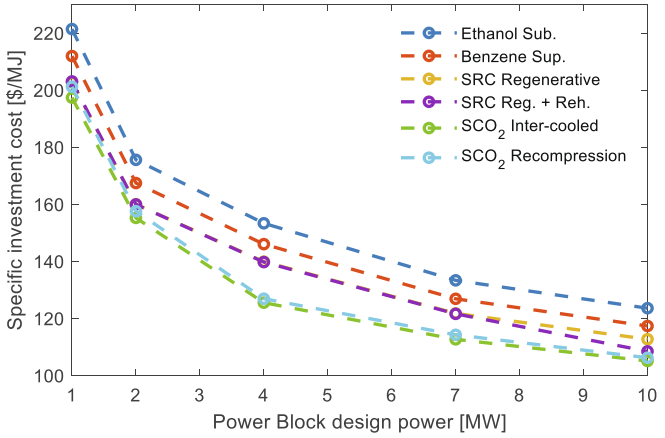

Fig. 14. Specific investment cost sensitivity analysis for the power block size.

Furthermore, there are two aspects that allows to have lower prices of the discharge portion of the system: 1) the use of an adiabatic carbonator (thanks to the simple component design); 2) extending the operation period imposed to the same subsystem, which makes possible to reduce the size of any component involved in the process.

Finally, in order to demonstrate that the indirect integration of power blocks based on supercritical carbon dioxide is economically convenient even for higher CSP plant sizes, a sensitivity analysis on the thermal cycle rated power is carried out. Fig. 14 shows that the sCO_2 power blocks advantage is not only maintained but even improved, reaching in some cases a relative improvement of the specific investment cost value equal to 22%. Increasing the plant size by one order of magnitude allows nearly halving the specific investment cost, although the parameter seem to have an asymptotic trend. In qualitative terms, the order of convenience of each integration alternative remains unchanged for all the cases evaluated in the sensitivity analysis.

Although the maximum size considered in the sensitivity analysis should seem not particularly high, it must be remembered that the operation time of discharging process is set to 24 h. Consequently, even small power blocks require high component sizes at the charging process (i.e. calciner sizes between 110 MW_{th} and 180 MW_{th} for thermal cycles of 10 MW_e). However, a possible way to extrapolate the specific investment cost (ic) for higher sizes is proposed in Eq. (46). It is based on the simplifying hypothesis that the cost of any plant section changes, according to the system size, with a power law and, in particular, with the same exponent of the most expensive component in the plant portion. Defining the Size Ratio (SR) as the ratio between the two sizes of plant 2 and plant 1, with Eq. (46) is possible to extrapolate the specific investment cost of plant 2 (ic_2) starting from investment costs of power block, carbonator side, calciner side, solar side and daily energy production of plant 1 ($IC_{PB/CarbS/ClcS/SolS}$ and E respectively).

$$ic_2 \cong \frac{IC_{PB1}\cdot SR^{0.684} + IC_{CarbS1}\cdot SR^{0.67} + IC_{ClcS1}\cdot SR^{0.48} + IC_{SolS1}\cdot SR^{-0.298}}{E_1\cdot SR} \quad (46)$$

6. Conclusions

According to authors knowledge, a complete economic analysis for the Calcium-Looping indirect integration in a central tower CSP plant is lacking in scientific literature. The present paper is devoted to the study and comparison (both in energy and economic terms) of this system. The power block considered are Organic Rankine Cycles, Steam Rankine Cycles and supercritical CO_2 Brayton cycles. A coherent methodology for the simulation of the calciner side that takes into account the intrinsic time dependence of its operation is adopted. Optimal operating conditions for the charging process are obtained through pinch analysis for both the calciner and carbonator sides. The HENs are designed taking into account the technical constraints affecting this kind of technology. In order to perform an economic analysis of the complete plant, suitable cost functions are collected from scientific literature and, when not found, are properly created. Not only the components investment costs are estimated, but economic optimizations are carried out for two important aspects related to the plant sections devoted to the perform the calcination reaction. Those are: a) the most convenient $CaCO_3$ split ratio for the solids preheating; b) the optimal dimensioning of components included in the solar side (heliostat field, central tower) and calciner side (reactor, HEN, compressors), in order to find the least expensive configuration able to satisfy the discharge process requirements.

Results obtained show that the best energy performances are achieved with sCO_2 power blocks (more than 19% for the design day), although steam Rankine cycles have simpler plant layouts. The outcomes of economic analysis show that thermal cycles based on supercritical carbon dioxide represent the best option for indirect integration even in economic terms. In all the cases investigated, the solar and calciner sides constitute a great part of the total capital investment (up to 86%). For this reason, the cost reduction occurring at the charge plant section caused by the adoption of very performing power blocks is such consistent that the integration of expensive sCO_2 power cycles (with prices nearly three times higher than ORC/SRC) is convenient. The storage turbine and CO_2 blower belonging to the carbonator side play an important role in the specific investment cost calculation, being even able to penalize the layout with the lower total capital requirement. Total plant efficiency and cost are both extremely important benchmarks to compare the investigated alternatives. However, it is fundamental to assume a normalized parameter in order to make a coherent economic analysis. In fact, it is shown that a normalized parameter can lead to different conclusion than the ones suggested by the two former indicators. Finally, is demonstrated that the sCO_2 thermal cycles convenience is guarantee even for higher CSP plant sizes.

The methodology exposed in the present paper for the calciner side simulation, the cost functions collected and the results obtained from the energy and economic analysis represent a solid base for further studies. Future work can be focused on a) assuming a larger variety of sCO_2 thermal cycles layouts; b) including the possibility to feed the power block with a heat transfer performed directly on the carbonator wall and c) evaluating the impact of these configurations on both the system performance and investment cost. These aspects are enough to justify the extension of the investigation with a companion paper (Part 2).

CRediT authorship contribution statement

U. Tesio: Conceptualization, Methodology, Visualization, Writing - original draft, Writing - review & editing. **E. Guelpa:** Conceptualization, Methodology, Formal analysis. **V. Verda:** Conceptualization, Methodology, Project administration, Funding acquisition.

Declaration of Competing Interest

The authors declare that they have no known competing financial interests or personal relationships that could have appeared to influence the work reported in this paper.

Acknowledgement

This work has been conducted within the European Project SOCRATCES (SOlar Calcium-looping integRAtion for Thermo-Chemical Energy Storage) GA 727348.

References

[1] S. J. S. T. L. M. Chen WY., "International Efforts to Combat Global Warming," in Handbook of Climate Change Mitigation, Springer, 2012, pp. 89-120.
[2] Oates W, Portney P. Economic incentives and the containment of global warming. East Econ J 1992;18:85–98.
[3] United Nations, "Framework Convention on Climate Change. Adoption of the Paris Agreement," 2015.
[4] SunShot Initiative - Solar Energy Technologies Office - U.S. Department of Energy, Tackling Challenges In Solar: 2014 Portfolio, 2014.
[5] International Energy Agency, "Technology roadmap solar thermal electricity," 2014.
[6] Tasbirul Islam M, Huda N, Abdullah A, Saidur R. A comprehensive review of state-of-the-art concentrating solar power (CSP) technologies: current status and research trends. Renew Sustain Energy Rev 2018;91:987–1018.
[7] Gauché P, Rudman J, Mabaso M, Landman W, von Backström T, Brent A. System value and progress of CSP. Sol Energy 2017;152:106–39.
[8] Pelay U, Luo L, Fan Y, Stitou D, Rood M. Thermal energy storage systems for concentrated solar power plants. Renew Sustain Energy Rev 2017;79:82–100.
[9] González-Roubaud E, Pérez-Osorio D, Prieto C. Review of commercial thermal energy storage in concentrated solar power plants: Steam vs. molten salts. Renew Sustain Energy Rev 2017;80:133–48.
[10] Peiró G, Prieto C, Gasia J, Jové A, Miró L, Cabeza L. Two-tank molten salts thermal energy storage system for solar power plants at pilot plant scale: Lessons learnt and recommendations for its design, start-up and operation. Renewable Energy 2018;121:236–48.
[11] Fernández A, Gomez-Vidal J, Oró E, Kruizenga A, Kruizenga A, Solé A, et al. Mainstreaming commercial CSP systems: a technology review. Renewable Energy 2019;140:152–76.
[12] Prieto C, Cabeza L. Thermal energy storage (TES) with phase change materials (PCM) in solar power plants (CSP). Concept and plant performance. Appl Energy 2019;254:113646.
[13] Prieto C, Cooper P, Fernández I, Cabeza L. Review of technology: thermochemical energy storage for concentrated solar power plants. Renew Sustain Energy Rev 2016;60:909–29.
[14] Office Of Energy Efficiency & Renewable Energy, "Concentrating Solar Power: Efficiently Leveraging Equilibrium Mechanisms for Engineering New Thermochemical Storage," [Online]. Available: https://www.energy.gov/eere/solar/concentrating-solar-power-efficiently-leveraging-equilibrium-mechanisms-engineering-new. [Accessed 2019].
[15] "Socratces Project | Energy Storage Technologies Viable & Sustainable," [Online]. Available: https://socratces.eu/. [Accessed 2019].
[16] "SolarPACES: Home," [Online]. Available: https://www.solarpaces.org/. [Accessed 2019].
[17] Bioazul, "Deliverable D8.1 - First Innovation Evaluation report," 2018.
[18] Ervin G. Solar heat storage using chemical reactions. J Solid State Chem 1977;22:51–61.
[19] Kuravi S, Trahan J, Goswami D, Rahman M, Stefanakos E. Thermal energy storage technologies and systems for concentrating solar power plants. Prog Energy Combust Sci 2013;39:285–319.
[20] P. Sánchez Jiménez, A. Perejón, A. Benítez Guerrero, J. Valverde, C. Ortiz and L. Pérez Maqueda, "High-performance and low-cost macroporous calcium oxide based materials for thermochemical energy storage in concentrated solar power plants," Applied Energy, vol. 235, pp. 543-552, Feb. 2019.
[21] Ortiz C, Valverde J, Chacartegui R, Perez-Maqueda L. Carbonation of Limestone Derived CaO for Thermochemical Energy Storage: From Kinetics to Process Integration in Concentrating Solar Plants. ACS Sustainable Chem Eng 2018;6:6404–17.
[22] Barin I. Thermochemical Data of Pure Substances. VCH; 1995.
[23] Arias B, Abanades J, Grasa G. An analysis of the effect of carbonation conditions on CaO deactivation curves. Chem Eng J Feb 2011;167:255–61.
[24] Cormos C-C, Petrescu L. Evaluation of calcium looping as carbon capture option for combustion and gasification power plants. Energy Procedia 2014;51:154–60.
[25] Alonso M, Rodríguez N, González B, Murillo R, Abanades J. Carbon dioxide capture from combustion flue gases with a calcium oxide chemical loop. Experimental results and process development. Int J Greenhouse Gas Control 2010;4:167–73.
[26] Benitez-Guerrero M, Sarrion B, Perejon A, Sanchez-Jimenez P, Perez-Maqueda L, Valverde JM. Large-scale high-temperature solar energy storage using natural minerals. Sol Energy Mater Sol Cells 2017;168:14–21.
[27] Chacartegui R, Alovisio A, Ortiz C, Valverde J, Verda V, Becerra J. Thermochemical energy storage of concentrated solar power by integration of the calcium looping process and a CO2 power cycle. Appl Energy 2016;173:589–605.
[28] Alovisio A, Chacartegui R, Ortiz C, Valverde J, Verda V. Optimizing the CSP-Calcium Looping integration for Thermochemical Energy Storage. Energy Convers Manage Mar. 2017;136:85–98.
[29] Ortiz C, Chacartegui R, Valverde J, Alovisio A, Becerra J. Power cycles integration in concentrated solar power plants with energy storage based on calcium looping. Energy Convers Manage Mar. 2017;149:815–29.
[30] Kemp I. Pinch Analysis and Process Integration. Butterworth-Heinemann; 2007.
[31] U. Tesio, E. Guelpa, C. Ortiz, R. Chacartegui and V. Verda, "Optimized synthesis/design of the carbonator side for direct integration of Thermochemical Energy Storage in size Concentrated Solar Power," Energy Conversion and Management: X, no. 100025, 2019.
[32] Ortiz C, Romano M, Valverde J, Binotti M, Chacartegui R. Process integration of Calcium-Looping thermochemical energy storage system in concentrating solar power plants. Energy 2018;155:535–51.
[33] Edwards S, Materić V. Calcium looping in solar power generation plants. Sol Energy 2012;86:2494–503.
[34] Karasavvas E, Panopoulos K, Papadopoulou S, Voutetakis S. Design of an integrated CSP-calcium looping for uninterrupted power production through energy storage. Chem Eng Trans 2018;70:2131–6.
[35] Ortiz C, Valverde J, Chacartegui R, Perez-Maqueda L, Giménez P. The Calcium-Looping (CaCO3/CaO) process for thermochemical energy storage in concentrating solar power plants. Renew Sustain Energy Rev 2019;113.
[36] Rolfe A, Huang Y, Haaf M, Rezvani S, Dave A, Hewitt NJ. Techno-economic and environmental analysis of calcium carbonate looping for CO2 capture from a pulverised coal-fired power plant. Energy Procedia 2017;142:3447–53.
[37] Tang Y, You F. Life cycle environmental and economic analysis of pulverized coal oxy-fuel combustion combining with calcium looping process or chemical looping air separation. J Cleaner Prod 2018;181:271–92.
[38] Cormos C-C. Economic evaluations of coal-based combustion and gasification power plants with post-combustion CO2 capture using calcium looping cycle. Energy 2014;78:665–73.
[39] Siefert N, Chang B, Litster S. Exergy and economic analysis of a CaO-looping gasifier for IGFC–CCS and IGCC–CCS. Appl Energy 2014;128:230–45.
[40] Fernández R, Ortiz C, Chacartegui R, Valverde JM, Becerra JA. Dispatchability of solar photovoltaics from thermochemical energy storage. Energy Convers Manage 2019;191:237–46.
[41] Stein W, Buck R. Advanced power cycles for concentrated solar power. Sol Energy 2017;152:91–105.
[42] E. Guelpa, U. Tesio and V. Verda, "DELIVERABLE D4.2 - Power cycles: schemes, models, analysis," SOlar Calcium-looping integRAtion for Thermo-Chemical Energy Storage, 2019.
[43] Toffolo A, Lazzaretto A, Morandin M. The HEATSEP method for the synthesis of thermal systems: An application to the S-Graz cycle. Energy 2010;35:976–81.
[44] "SysCAD: Plant Simulation Software," [Online]. Available: https://www.syscad.net/. [Accessed 2019].
[45] M. Chase, NIST-JANAF thermochemical tables. Fourth edition., American Institute of Physics, 1998.
[46] I. Bell, J. Wronski, S. Quolin and V. Lemort, "Welcome to CoolProp — CoolProp 6.3.0 documentation," [Online]. Available: http://www.coolprop.org/. [Accessed 2019].
[47] G. Zsembinszki, A. Solé, C. Barreneche, C. Prieto, . I. Fernández and L. Cabeza, "Review of Reactors with Potential Use in Thermochemical Energy Storage in Concentrated Solar Power Plants," Energies, vol. 11, no. 2358, 2018.
[48] G. Moumin, S. Tescari, P. Sundarraj, L. de Oliveira, M. Roeb and C. Sattler, "Solar treatment of cohesive particles in a directly irradiated rotary kiln," Solar Energy, vol. 182, pp. 480-490, 2019.
[49] Meier A, Bonaldi E, Cella G, Lipinski W, Wuillemin D. Solar chemical reactor technology for industrial production of lime. Sol Energy 2006;80:1355–62.
[50] Moumin G, Ryssel M, Zhao L, Markewitz P, Sattler C, Robinius M, et al. CO2 emission reduction in the cement industry by using a solar calciner. Renewable Energy 2020;145:1578–96.
[51] Ho C. "A new generation of solid particle and other high-performance receiver designs for concentrating solar thermal (CST) central tower systems," in *Advances in Concentrating Solar Thermal Research and Technology*. Woodhead Publishing 2017:107–28.
[52] Ho CK. A review of high-temperature particle receivers for concentrating solar power. Appl Therm Eng 2016;109:958–69.
[53] Ferrara G, Lanzini A, Leone P, Ho MT, Wiley DE. Exergetic and exergoeconomic analysis of post-combustion CO2 capture using MEA-solvent chemical absorption. Energy 2017;130:113–28.
[54] Kurtulus K, Coskun A, Ameen S, Yilmaz C, Bolatturk A. Thermoeconomic analysis of a CO2 compression system using waste heat into the regenerative organic Rankine cycle. Energy Convers Manage 2018;168:588–98.
[55] Qiu Y, He Y-L, Du B-C. A comprehensive model for analysis of real-time optical performance of a solar power tower with a multi-tube cavity receiver. Appl Energy 2017;185:589–603.
[56] "European Central Bank," [Online]. Available: https://www.ecb.europa.eu/. [Accessed 2019].
[57] P. Ahmadi, Modeling, Analysis and Optimization of Integrated Energy Systems for Multigeneration Purposes, 2013.
[58] M. Carlson, B. Middleton and C. Ho, "Techno-Economic Comparison of Solar-Driven SCO2 Brayton Cycles Using Component Cost Models Baselined With Vendor Data and Estimates," in Proceedings of the ASME 2017 11th International Conference on Energy Sustainability , 2017.
[59] S. Michalski, D. Hanak and V. Manovic, "Techno-economic feasibility assessment of calcium looping combustion using commercial technology appraisal tools," Journal of Cleaner Production, vol. 219, p. 540e551, 2019.
[60] Albrecht K, Ho C. Design and operating considerations for a shell-and-plate, moving packedbed, particle-to-sCO2 heat exchanger. Sol Energy 2019;15:331–40.
[61] Nazari N, Heidarnejad P, Porkhial S. Multi-objective optimization of a combined steam-organic Rankine cycle based on exergy and exergo-economic analysis for

waste heat recovery application. Energy Convers Manage 2016;127:366–79.
[62] Bayon A, Bader R, Jafarian M, Fedunik-Hofman L, Sun Y, Hinkley J, et al. Techno-economic assessment of solid–gas thermochemical energy storage systems for solar thermal power applications. Energy 2018;149:473–84.
[63] M. Jonemann, "Advanced Thermal Storage System with Novel Molten Salt," National Renewable Energy Laboratory, 2013.
[64] AK Steel, "304/304L stainless steel, product data bulletin," 2016.
[65] De Lena E, Spinelli M, Gatti M, Scaccabarozzi R, Campanari S, Consonni S, et al. Techno-economic analysis of calcium looping processes for low CO2 emission cement plants. Int J Greenhouse Gas Control 2019;82:244–60.
[66] K. W. Battleson, "Solar power tower design guide: solar thermal central receiver power systems. A source of electricity and/or process heat," Sandia National Labs, 1981.
[67] Meier A, Gremaud N, Steinfeld A. Economic evaluation of the industrial solar production of lime. Energy Convers Manage 2005;46:905–26.